NUCL SCI TECH (2017) 28:176
https://doi.org/10.1007/s41365-017-0326-4

Damage produced on GaN surface by highly charged Kr^{q+} irradiation

Li-Qing Zhang[1,2] · Chong-Hong Zhang[1] · Chao-Liang Xu[1,2] · Heng-Qing Zhang[1,2] · Yi-Tao Yang[1] · Jin-Yu Li[1] · Hui-Ping Liu[1] · Zhao-Nan Ding[1] · Ting-Xing Yan[1,2]

Received: 27 February 2017 / Revised: 22 May 2017 / Accepted: 2 June 2017 / Published online: 16 November 2017

Abstract Surface morphology, compositions, microstructure and optical properties of GaN film irradiated by highly charged Kr^{q+} ($q = 23$, 15, 11) in two geometries to a fluence of 1×10^{15} kr^{q+}/cm^2 were studied using AFM, XPS, PL, Raman scattering and UV–visible spectroscopy. The AFM observation shows that the irradiated GaN area is a swollen terrace. The swelling rate increased with the charge state (potential energy). For the same charge state, the swelling rate of tilted incidence was greater than that for normal incidence. The XPS measurements reveal that N deficiency, Ga enrichment and Ga–O and Ga dangling bonds generated on the irradiated GaN surface increased with the charge state, and more N was lost for normal incidence than that for tilted incidence. The UV–Vis results show that the transmittance decreased with increasing charge state. For the same charge state, the transmittance for tilted incidence is higher than that for normal incidence. The PL spectra present that, with increasing charge state, the YL band intensity decreased, with a blueshift in its peak position; while the NBE peak intensity increased first and then reduced, and a blue luminescence band appeared. A rapid quenching of both the YL and the NEB for normal incidence was observed. Raman spectra display that screw dislocations perhaps were produced near the surface for normal incidence.

Keywords GaN · Highly charged Krypton ion · AFM · XPS · UV–Vis transmittance spectra · PL · Raman spectra

1 Introduction

Highly charged ions (HCIs) have been studied for three decades. Hollow atom formation, secondary electron emission and potential sputtering were observed due to the transient release of the potential energy. HCI potential energy deposition was confined in a nanometer-sized volume close to the target surface, in a femtosecond time scale via electron exchanges, causing a permanent nano-structure deformation on the material surface. Nano-structure modifications on insulator and semiconductor surfaces tailored by HCIs were extensively reported [1–6]. Correspondingly, HCIs have been proposed as a tool for surface deformations and analysis on the nanometer scale [7].

GaN-based materials are promising semiconductor widely used in optoelectronic devices (light-emitting diodes, laser diodes and UV detector, etc.) due to their superior properties, such as wide band gap, high electron mobility, high saturated electron drift velocity, high breakdown electric field, tolerance to the high temperature, resistance to the radiation. In response to the exploding demands for larger storage capacities, faster data transfer rate and lower energy consumption, GaN-based devices have to be downsized in the scope and integrated in the

This work was supported by the National Natural Science Foundation of China (Nos. 11675231, 91426304 and 11105191), the National Magnetic Confinement Fusion Program (No. 2011GB108003) and the National Basic Research Program of China (No. 2010CB832904).

✉ Chong-Hong Zhang
c.h.zhang@impcas.ac.cn

Li-Qing Zhang
liqingzhang07@impcas.ac.cn

[1] Institute of Modern Physics, Chinese Academy of Sciences, Lanzhou 730000, China

[2] University of Chinese Academy of Sciences, Beijing 100049, China

circuit continuously. HCIs have a wide application prospect in fabrications of nanoscale GaN-based devices, such as surface nano-patterning, erosion, purification, roughness, analysis. In an early paper, we reported HCI-induced nano-structure deformations in GaN surface [8]. In this paper, GaN samples are irradiated by 460 keV Kr^{q+} ($q = 23$, 15, 11) beams in tilted and normal incidence to a fluence of 1×10^{15} kr^{q+}/cm^2 and are characterized by atomic force microscopy (AFM), X-ray photoelectron spectroscopy (XPS), UV–visible spectroscopy (UV–Vis), Raman scattering and photoluminescence spectroscopy (PL).

2 Experimental section

N-type GaN films of about 2 μm thickness were grown on (0001) sapphire substrates by metal–organic chemical vapor-deposition (MOCVD). Specimens sized at 10 mm × 10 mm were irradiated with 460 keV Kr^{q+} to $1 \times 10^{15}/cm^2$ at room temperature (RT) in 10^{-7} mbar vacuum. The 460 keV refers to the pure kinetic energy, not the total of kinetic + potential energy. The irradiation was performed in normal incidence and tilted incidence at 60° from the surface normal. During irradiation, each specimen was partially masked with a TEM 3-mm fine square copper mesh in an effort to compare the irradiated and un-irradiated regions. Kr^{q+} ions were extracted from the ion source at the atomic physics experimental platform with the terminal voltage of 320 kV in Institute of Modern Physics (IMP), Chinese Academy of Sciences. The beam intensity was up to 0.4 μA.

The irradiated specimens were inspected by tapping-mode AFM, XPS, PL, Raman scattering, and UV–Vis in ambient air. The AFM (NanoscopyIII a, Digital Instrument) was of 12 μm × 12 μm scan range, 15 nm scan scope along z-axis, 10-V maximal operation voltage, and 1.0 Hz scan frequency. The XPS (PHI-5702 ESCA, PerkinElmer Inc.) was operated in a vacuum chamber of 5×10^{-9} torr. The dual anode X-ray source, working at 14 kV with 250 W output power, provides Mg Kα (1253.6 eV) and Al Kα (1486.6 eV). For an accurate determination of the spectral peak position, the C1s binding energy was assigned at 284.8 eV. Spectra were obtained using the Al Kα ray and pass energy of analyzer is 29.3 eV; spectral peak position of Ga3d was determined by referencing to the C1s spectra.

The PL spectra were recorded using xenon lamp of 354 nm (3.503 eV) with a maximum input power of 30 mW. Integration time was 100 ms, the width of detector slits was 100 μm, and the spectral resolution was 0.1 nm. The UV–Vis measurements were taken using a Lambda 900 UV/VIS/NIR spectroscope (PerkinElmer Inc.). Wolfram and deuterium lamps were used as the incident light. The spectral resolution was 0.1 nm. The transmittance spectra are recorded from 200 to 1000 nm wave length region. Raman scattering spectra were measured on a JY HR800 micro-Raman system with a confocal microscopy system. The spectra were taken at room temperature with the 632.8-nm excitation of a He–Ne laser in a backscattering geometry, where the scattered light propagated in a direction parallel to the c axis of GaN epilayer. The laser beam focused on the sample surface was about 2 μm in diameter. To avoid laser heating and local annealing effects, the He–Ne laser power was kept below 2 mW. The spectral resolution was 0.65 cm^{-1}.

3 Results and discussion

Figure 1 shows the 2D AFM image and its local cross section graph of a GaN sample irradiated at the normal incidence. The cross section graph characterizes a surface height profile and measures surface height along a certain direction in a small region. The un-irradiated region (A in Fig. 1a) of the GaN film has a typical dislocation-medicated surface morphology, being made up of an array of terraces, while the irradiated region (B in Fig. 1a) has a swollen surface, with an obvious step between the two regions, in a step height of 1.5 ± 10% nm.

Figure 2 shows the dependence of surface swelling rate on charge state of the Kr^{q+} ions for the GaN samples irradiated in normal and 60° incidence. The swelling rate was defined as the formed step height over the ions range. It increased with the charge state, due to higher potential energy deposition. The step heights were 2.0, 1.5 and 0 nm for Kr^{23+}, Kr^{15+} and Kr^{11+} at 60° incidence, respectively, while they were 1.5, 1.0 and 0.1 nm for Kr^{23+}, Kr^{15+} and Kr^{11+} at normal incidence, respectively. The trajectory range of 460 keV Kr^{q+} in GaN film is about 140 nm. At the same charge state, the swelling rate for tilted incidence is larger than that for normal incidence. This is probably ascribed to the deposition of potential energy only near the surface due to the larger deposition area for tilted incidence.

Figure 3 shows Ga $3d_{5/2}$ XPS spectra of the GaN samples irradiated in two geometries. Table 1 shows the binding energy of the Ga–N bond and the relative content of Ga–N, Ga–Ga and Ga–O bond of the GaN samples irradiated in normal incidence (N) and tilted incidence (T). After irradiation, the peak intensity of Ga–N bond (19.8 eV [9]) decreased drastically and a new contribution was evident indicating that the relative content of Ga–N bond reduced and new bonds produced.

For tilted incidence, the main peak shifted toward higher binding energy generally, indicating that the binding

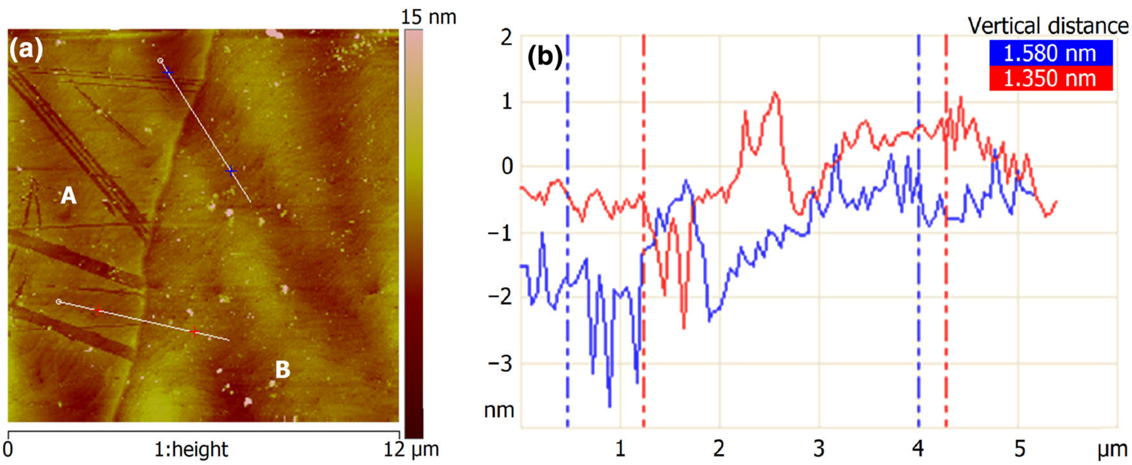

Fig. 1 (Color online) AFM image and its local cross section graph of the GaN film irradiated at normal incidence. The A and B denote the un-irradiated and irradiated regions, respectively. A step between the two regions can be seen obviously

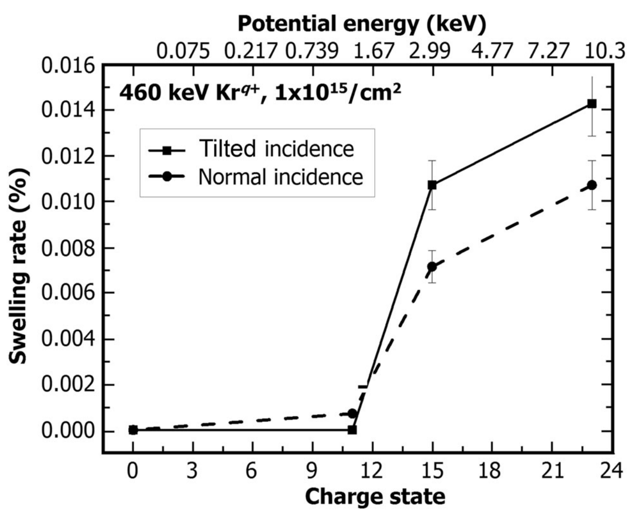

Fig. 2 Surface swelling rate as a function of the charge state (potential energy) of the GaN samples irradiated in two geometries

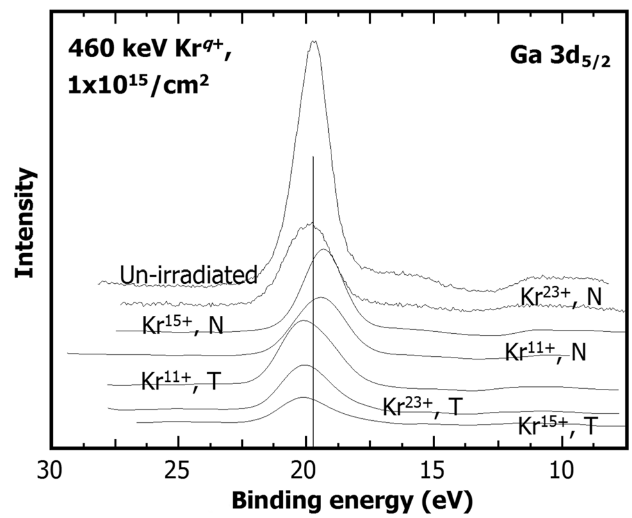

Fig. 3 Ga $3d_{5/2}$ XPS of GaN samples irradiated in normal (N) and 60° (T) incidence. All spectra were shifted vertically for clarity

energy of Ga–N increased and its length shortened due to the loss of the N atom and a migration of the O toward the N sites. The Ga–O bond at 21.6 eV can be seen in the spectra [9]. Also, with increasing charge state (potential energy), the relative content of Ga–O bond increased and Ga–N bond content decreased.

For normal incidence, the main peak shifted toward lower binding energy, indicating the generation of Ga dangling bonds (Ga_{DBs}) or Ga–Ga bond (17.5 eV [9]), and the decrease in Ga–N bond content. At the same charge state, the relative content of the Ga–N bond for the 60° incidence was higher than that for normal incidence, indicating that the normal incidence produced heavier surface damage than the 60° incidence. This attributes to the shorter interaction time and larger potential energy deposition density near the surface for normal incidence. The interaction between the HCI and the solid surface starts from a critical distance r_c above the surface. From this point, electrons are resonantly captured from the valence band of the material into highly excited Rydberg states of the approaching ion. The area of potential energy deposition for the 60° incidence is larger than that for normal incidence. In short, the Ga $3d_{5/2}$ XPS spectra reveal N depletion and Ga enrichment after Kr^{q+} irradiation due to smaller adsorption energy of N [10] and larger mobility of Ga [11].

From the UV–visible spectra of GaN film irradiated in two geometries (Fig. 4), the following information can be obtained. For the un-irradiated GaN film, the transmission spectrum exhibits a sharp absorption edge. GaN has high absorption coefficient of the order of 10^5 cm^{-1} and low transmittance. After irradiation, the transmittance of irradiated samples decreased, and the band edge transmittance

Table 1 Ga–N binding energy, Ga–N, Ga–Ga and Ga–O relative content of GaN irradiated by 460 keV Kr^{q+} to 1×10^{15} Kr^{q+}/cm^2 in two geometries

Charge state/potential energy (keV)		Ga–N binding energy (eV)	Relative content (%)		
			Ga–N	Ga–Ga	Ga–O
11/1.315	N	19.45	90.95	4.99	4.06
	T	19.96	99.64	0	0.36
15/2.994	N	19.35	90.65	5.66	3.69
	T	20.01	93.05	6.57	0.38
23/9.205	N	19.82	83.92	4.64	11.44
	T	19.99	92.95	6.53	0.52
Un-irradiated		19.80	100	0	0

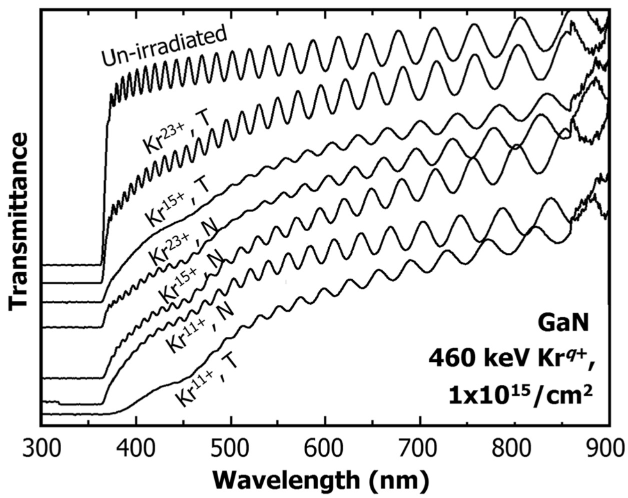

Fig. 4 UV–visible spectra of GaN irradiated in normal (N) and 60° (T) incidence. All spectra were shifted vertically for clarity

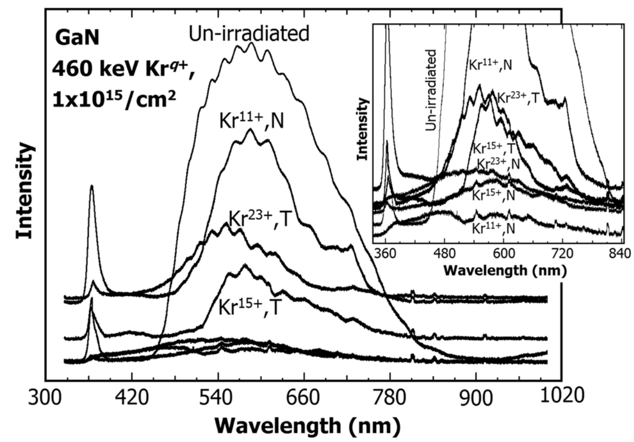

Fig. 5 PL spectra and the local amplification of GaN irradiated in normal (N) and 60° (T) incidence. All spectra were shifted vertically for clarity

decreased slowly. These ascribe to the production of defects. The transmittance for the Kr^{23+} ion irradiation was higher than those for Kr^{15+} and Kr^{11+} ion irradiation. The transmittance for the 60° incidence was higher than that for normal incidence, due to the severe damage caused by the normal incidence to the GaN target. This is consistent with the XPS analysis. However, for Kr^{15+} and Kr^{11+} ion irradiation, transmittance for tilted incidence was lower than that for normal incidence. These phenomena could be related to the formation of a different type of defect, such as cluster of point defects. The absorption efficiency of defect cluster is lower than the single absorption center [12]. On the other hand, extended defects (screw dislocations and dislocation loops) could be produced near the surface due to the release of stress, which could absorb the point defects and defects clusters, resulting in a respective change in transmittance spectra after irradiation under different conditions.

The PL spectra of the GaN irradiated in two geometries are shown in Fig. 5. The insert shows the partial amplified spectra lines. After irradiation, the intensity of the near-band-edge emission (NBE) ($\sim$ 360 nm) increased first and then decreased, while the intensity of the yellow luminescence (YL) band (480–800 nm) decreased evidently, with a blueshift of peaks position. The near-band-edge peak at 363 nm (3.413 eV) is a neutral-donor-bound exciton (D_0, X) peak, which attributes to nitrogen vacancies. Nitrogen vacancies on the GaN surface behave as native donors and can indeed contribute to the stronger donor peak observed in the near-band-edge luminescence [13]. The YL at 563 nm (2.2 eV) was attributed to the combination between shallow donors (Si_{Ga}, O_N [14] or C_{Ga} [15]) and deep acceptors (V_{Ga}) [16–18]) or recombination of some complex defects (O_N-V_{Ga}) [17]. The preferential loss of N caused an increase in the near-band-edge emission intensity for irradiation of the lowest charge state (Kr^{11+}). A blueshift of the YL was attributed to the formation of complex defects (O_N-V_{Ga}) after irradiation [14, 17], being consistent with the XPS results. With increasing charge state, the annihilation of the YL and the NBE was attributed to various defects generation and trapping of carriers at ions-produced defects [19]. For Kr^{15+} and Kr^{23+} irradiations, a rapid quenching of the YL band and NBE emission for normal incidence was found in contrast to the 60° incidence due to the occurrence of heavier damages for

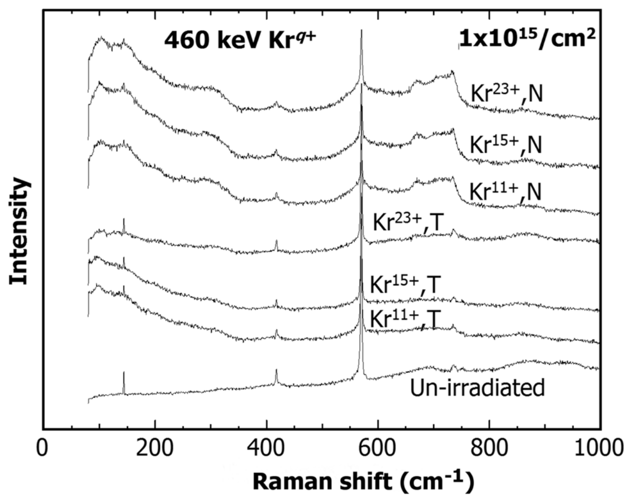

Fig. 6 Raman scattering spectra of GaN irradiated in normal (N) and 60° (T) incidence. All spectra were shifted vertically for clarity

normal incidence, being consistent with the XPS and UV–Vis analyses. A decrease in the transmittance and an annihilation of the YL and the NEB are owing to the generation of various defects in the band gap due to the irradiation. Moreover, as the YL and NBE disappear, the blue luminescence band centered near 400 nm (3.1 eV) arises. This ascribes to the transition of sallow donor (O_N) to the deep acceptor (V_{Ga}–O_N) [14].

Figure 6 shows Raman scattering spectra of the GaN irradiated in two geometries. For all the samples, the peak near 144, 570, 740 cm^{-1} is the first-order phonon frequencies of E_2 (low), E_2 (high) and A_1 (LO), respectively, reflecting the characteristics of the hexagonal crystal phase GaN [20]. After irradiation, peaks at 300 and 670 cm^{-1} attributed to DARS (disorder-activated Raman scattering) related to Ga and N vacancies arise, and step-like feature between 100 and 200 cm^{-1} is observed for normal incidence, because GaN lattices are disordered which leads to a loss of translational periodicity, hence the relaxation of $q = 0$ conservation [21, 22]. Furthermore, the A_1 (LO) at 740 cm^{-1} broadens with asymmetric line shape due to the participation of a silent vibration mode (E_1) under this scattering geometry for normal incidence, indicating occurrence of the rotation and the tilt of lattices plane [23]. Therefore, screw dislocations and dislocation loops perhaps were produced near the surface.

4 Conclusion

Surface morphology, composition, microstructure and optical characterization of GaN film irradiated by 460 keV Kr^{q+} ($q = 23, 15, 11$) to a fluence of 1×10^{15} Kr^{q+}/cm^2 in two geometries were investigated using AFM, XPS, PL, Raman scattering and UV–visible spectroscopy. Results show the irradiated GaN surface is a swelling terrace and the swelling rate increases with the increase in the charge state. Meanwhile, N deficiency, Ga enrichment, Ga–Ga and Ga–O bonds generation were observed on the irradiated GaN surface; N vacancies, Ga vacancies and screw dislocations also were produced for normal incidence. On the other hand, after irradiation, the transmittance and luminescence intensity decrease generally. And with the increase in the charge state, the transmittance increases, the YL band and the NBE were quenched and a blue luminescence band appears. Moreover, at the same charge state, the heavier surface damage was induced by normal incidence than by tilted incidence generally. More damage mechanisms need to further detect. These results may provide a reference for applications of HCI in GaN-based devices fields.

Acknowledgements The authors are grateful to Suzhou Institute of Nano-tech and Nano-bionics (SINANO) of Chinese Academy of Sciences for AFM measurements and to the team of the 320-kV platform in Institute of Modern Physics, Chinese Academy of Sciences.

References

1. A.S. El-Said, R.A. Wilhelm, R. Heller et al., Creation of surface nanostructures in Al_2O_3 by slow highly charged ions. Nucl. Instr. Methods B **317**, 170 (2013). https://doi.org/10.1016/j.nimb.2013.01.054
2. R. Heller, S. Facsko, R.A. Wilhelm et al., Defect mediated desorption of the KBr(001) surface induced by single highly charged ion impact. Phys. Rev. Lett. **101**, 096102 (2008). https://doi.org/10.1103/PhysRevLett.101.096102
3. M. Terada, N. Nakamura, Y. Nakai et al., Observation of an HCI-induced nano-dot on an HOPG surface with STM and AFM. Nucl. Instr. Methods B **235**, 452 (2005). https://doi.org/10.1016/j.nimb.2005.03.223
4. M. Tona, Y. Fujita, C. Yamada et al., Electronic interaction of individual slow highly charged ions with TiO_2(110). Phys. Rev. B. **77**, 155427 (2008). https://doi.org/10.1103/PhysRevB.77.155427
5. T.K. Chini, D.P. Datta, S.R. Bhattacharyya et al., Ripple formation on silicon by medium energy ion bombardment. J. Phys. Condens. Matter **21**, 224004 (2009). https://doi.org/10.1088/0953-8984/21/22/224004
6. F. Aumayr, H. Winter, Potential sputtering: one contribution of 11 to a Theme ‘Sputtering: past, present and future. Philos. Trans. R. Soc. Lond. **362**, 77 (2004). https://doi.org/10.1098/rsta.2003.1300
7. F. Aumayr, H.P. Winter, Slow highly charged ions—a new tool for surface nanostructuring. e-J. Surf. Sci. Nanotech. **1**, 171 (2003). https://doi.org/10.1380/ejssnt.2003.171
8. L.Q. Zhang, C.H. Zhang, Y.T. Yang et al., Potential energy threshold of surface erosion on GaN by impact of slow highly charged heavy ions. Nucl. Instr. Methods B **269**, 369 (2011). https://doi.org/10.1016/j.nimb.2010.11.043
9. D. Sadowska, A. Gladki, K. Mazur et al., Optimisation of the epi-ready semi-insulating GaAs wafer preparation procedure.

Vacuum **72**, 217 (2004). https://doi.org/10.1016/S0042-207X(03)00143-X
10. J. Neugebauer, T. Zywietz, M. Scheffler et al., Theory of surfaces and interfaces of group-III nitrides. Appl. Surf. Sci. **159–160**, 355 (2000). https://doi.org/10.1016/S0169-4332(00)00154-9
11. R.M. Feenstra, H. Chen, V. Ramachandran et al., Reconstructions of GaN and InGaN surfaces. Appl. Surf. Sci. **166**, 165 (2000). https://doi.org/10.1016/S0169-4332(00)00401-3
12. P. Musumeci, L. Calcagno, M.G. Grimaldi et al., Optical defects in ion damaged 6H-silicon carbide. Nucl. Instr. Methods B **116**, 327 (1996). https://doi.org/10.1016/0168-583X(96)00067-5
13. P. Perlin, T. Suski, H. Teisseyre et al., Towards the identification of the dominant donor in GaN. Phys. Rev. Lett. **75**, 296 (1995). https://doi.org/10.1103/PhysRevLett.75.296
14. C.B. Soh, S.J. Chua, H.F. Lim et al., Assignment of deep levels causing yellow luminescence in GaN. J. Appl. Phys. **96**, 1341 (2004). https://doi.org/10.1063/1.1757654
15. L. Dai, G.Z. Ran, J.C. Zhang et al., C and Si ion implantation and the origins of yellow luminescence in GaN. Appl. Phys. A **79**, 139 (2004). https://doi.org/10.1007/s00339-003-2384-1
16. T. Ogino, M. Aoki, Mechanism of yellow luminescence in GaN. Jpn. J. Appl. Phys. **19**, 2395 (1980). https://doi.org/10.1143/JJAP.19.2395
17. J. Neugebauer, C.G. Van de Walle, Gallium vacancies and the yellow luminescence in GaN. Appl. Phys. Lett. **69**, 503 (1996). https://doi.org/10.1063/1.117767
18. K. Saarinen, T. Laine, S. Kusima et al., Observation of native Ga vacancies in GaN by positron annihilation. Phys. Rev. Lett. **79**, 3030 (1997). https://doi.org/10.1103/PhysRevLett.79.3030
19. M. Fehrer, S. Einfeldt, U. Birkle et al., Impact of defects on the carrier transport in GaN. J. Cryst. Growth. **189/190**, 763 (1998). https://doi.org/10.1016/S0022-0248(98)00284-X
20. VYu. Davydov, Y.E. Kitaev, I.N. Goncharuk et al., Phonon dispersion and Raman scattering in hexagonal GaN and AlN. Phys. Rev. B. **58**, 12899 (1998). https://doi.org/10.1103/PhysRevB.58.12899
21. W. Limmer, W. Ritter, R. Sauer et al., Raman scattering in ion-implanted GaN. Appl. Phys. Lett. **72**, 2589 (1998). https://doi.org/10.1063/1.121426
22. W. Pollard, Vibrational properties of amorphous GaN. J. Non-Cryst. Solids **283**, 203 (2001). https://doi.org/10.1016/S0022-3093(01)00461-6
23. T. Kozawa, T. Kachi, H. Kano et al., Raman scattering from LO phonon-plasmon coupled modes in gallium nitride. J. Appl. Phys. **75**, 1098 (1994). https://doi.org/10.1063/1.356492